FACULTEIT TOEGEPASTE WETENSCHAPPEN
DEPARTEMENT BURGERLIJKE BOUWKUNDE
AFDELING BOUWMECHANICA
KASTEELPARK ARENBERG 40
B-3001 HEVERLEE

KATHOLIEKE
UNIVERSITEIT
LEUVEN

Status

G. DE GRANDE, G. LOMBAERT, *High-speed train induced free field vibrations: in situ measurements and numerical modelling*, In N. Chouw and G. Schmid, editors, Proceedings of the International Workshop Wave 2000, Wave propagation, Moving load, Vibration reduction, pages 29-41, Ruhr University Bochum, Germany, December 2000, A.A. Balkema, Rotterdam.

IR. G. LOMBAERT
TEL. (+32 16)32 16 68 FAX (+32 16)32 19 88
E-mail: geert.lombaert@bwk.kuleuven.ac.be

High-speed train induced free field vibrations: in situ measurements and numerical modelling

G. Degrande & G. Lombaert
K.U.Leuven, Department of Civil Engineering, W. de Croylaan 2, B-3001 Heverlee

ABSTRACT: Homologation tests of the HST track between Brussels and Paris have been used to measure free field vibrations and track response during the passage of a Thalys HST at speeds varying between 223 km/h and 314 km/h. These experimental data are complementary to other data sets published in the literature and used in the present paper to validate a numerical model for high-speed train induced vibrations. Use is made of Krylov's prediction model, that is efficiently reformulated using the Betti-Rayleigh dynamic reciprocity theorem applied to moving loads. The model seems to offer good predictive capabilities for the low and high frequency contribution to the near field response.

1 INTRODUCTION

Six weeks before the inauguration of the HST track between Brussels and Paris in December 1997, the Belgian railway company has organized homologation tests during the passage of a Thalys HST at a speed varying between 160 and 330 km/h. As available experimental data are scarce, especially regarding the influence of the train speed on the vibration amplitudes, this opportunity has been taken to perform free field vibration measurements on the track and in the free field at distances varying from 4 m to 72 m (Degrande & Schillemans 1998, Degrande 2000). The in situ measurements have been performed near Ath, 55 km south of Brussels, where the train can reach maximum speed. The results obtained are complementary to in situ vibration measurements performed during the passage of the Thalys HST on the track Amsterdam-Utrecht in the Netherlands, at speeds between 40 and 160 km/h (Branderhorst 1997), to data reported by Auersch (1989) for the German ICE train at speeds varying between 100 and 300 km/h and to measurements with the X2000 train on the West Coast Line in Sweden (Adolfsson et al. 1999).

In a series of papers, Krylov (1994, 1995, 1998) has proposed an analytical prediction model for train induced vibrations. The quasi-static force transmitted by a sleeper is derived from the deflection curve of the track, modelled as a beam on an elastic foundation. Other excitation mechanisms (parametric excitation, wheel and rail roughness, rail joints and wheelflats) and through-soil coupling of the sleepers, as incorporated in more advanced track models (Knothe & Wu 1998, Van den Broeck & De Roeck 1996), are not accounted for. Krylov's original formulation uses Lamb's approximate solution for the Green's function of a halfspace and can be easily extended to incorporate the Green's functions of a layered halfspace (Degrande et al. 1998, Degrande 1999). It can also be made more efficient from a computational point of view, relying on the Betti-Rayleigh dynamic reciprocity theorem applied to moving loads (Lombaert & Degrande 2000).

The objectives of this paper are the following. First, the characteristics of the train, the track and the subsoil, as well as the experimental setup are briefly recapitulated. Second, the time history and the frequency content of the vertical response of the sleeper and the free field at various distances to the track are discussed. Third, a brief account is given of an efficient alternative for Krylov's prediction model. This results in the fourth objective of the paper, the comparison of the experimental results and the numerical predictions.

2 THE IN-SITU MEASUREMENTS

2.1 *The train*

Figure 1 shows the configuration of the Thalys HST, consisting of 2 locomotives and 8 carriages; the total length of the train is equal to 200.18 m. The locomotives are supported by 2 bogies and have 4 axles. The carriages next to the locomotives share one bogie with the neighbouring carriage, while the 6 other carriages share both bogies with neighbouring carriages. The total number of bogies equals 13 and, consequently, the number of axles on the train is 26. The carriage length L_t, the distance L_b between bogies, the axle distance L_a, the total axle mass M_t, the sprung axle mass M_s and the unsprung axle mass M_u of all carriages are summarized in table 1.

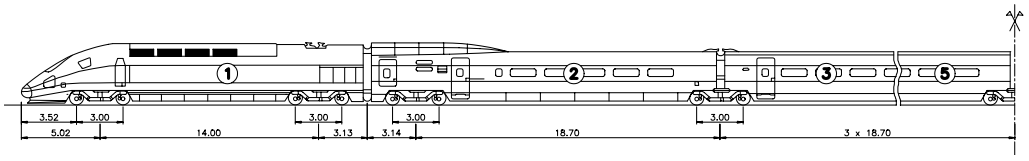

Figure 1: Configuration of the Thalys HST.

	# carriages	# axles	L_t [m]	L_b [m]	L_a [m]	M_t [kg]	M_s [kg]	M_u [kg]
Locomotives	2	4	22.15	14.00	3.00	17000	15267	1733
Side carriages	2	3	21.84	18.70	3.00	14500	12674	1830
Central carriages	6	2	18.70	18.70	3.00	17000	15170	1826

Table 1: Geometrical and mass characteristics of the Thalys HST.

2.2 *The track*

Continuously welded UIC 60 rails with a mass per unit length of $60\,\mathrm{kg/m}$ and a moment of inertia $I = 0.3038 \times 10^{-4}\,\mathrm{m}^4$ are fixed with a Pandroll E2039 rail fixation system on precast prestressed concrete monoblock sleepers with a length $l = 2.5\,\mathrm{m}$, a width $b = 0.285\,\mathrm{m}$, a height $h = 0.205\,\mathrm{m}$ (under the rail) and a mass of $300\,\mathrm{kg}$. Flexible rail pads with thickness $t = 0.01\,\mathrm{m}$ and a static stiffness of about $100\,\mathrm{MN/m}$, for a load varying between $15\,\mathrm{kN}$ and $90\,\mathrm{kN}$, are placed under the rail. The track is supported by a porphyry ballast layer (calibre 25/50, layer thickness $d = 0.3\,\mathrm{m}$), a limestone or porphyry layer (0/32, $d = 0.2\,\mathrm{m}$) and a limestone supporting layer (0/80 to 0/120, $d = 0.5 - 0.7\,\mathrm{m}$).

2.3 *The soil*

Cone penetration tests and triaxial tests on undisturbed samples taken from borehole experiments reveal the presence of a quaterny loam layer (0-1.5 m) on a transition layer (quaterny loam and/or an Ypresian clay, 1.5-4.0 m) on a tertiary Ypresian clay layer (4.0-12.0 m).

A spectral analysis of surface waves (SASW) has been performed to determine the dynamic soil characteristics of the site (Dewulf et al. 1996) and revealed the presence of a top layer with thickness $d = 1.4\,\text{m}$ and a shear wave velocity $C_s = 80.0\,\text{m/s}$ and a layer ($d = 1.9\,\text{m}$, $C_s = 133.0\,\text{m/s}$) on top of a halfspace ($C_s = 226.0\,\text{m/s}$), in good agreement with the layering revealed by the borehole experiments. The track is constructed in an excavation with a depth of a few meters, where the soil under the ballast has been stabilized. As the SASW test has been performed on the unexcavated soil away from the track, we may assume that the soil under the track is stiffer than the soft shallow layer revealed by the SASW test. In the subsequent calculations, a shear wave velocity $C_s = 100.0\,\text{m/s}$ will therefore be used for the top layer.

Based on a simplified analysis of the transient signals recorded during the SASW-test, a hysteretic material damping ratio $\beta^s = 0.03$ has been derived. In practice, material damping ratios are expected to decrease with depth and may be lower than the proposed value for deeper layers.

2.4 *The experimental setup*

Vertical accelerations have been measured at 14 locations (figure 2). On both tracks, a Dytran piezoelectric accelerometer was glued to the rail and the sleeper. In the free field, 10 seismic piezoelectric PCB accelerometers were placed at distances 4, 6, 8, 12, 16, 24, 32, 40, 56 and 72 m from the center of track 2. They were mounted on steel or aluminium stakes with a crucifix cross section to minimize dynamic soil-structure interaction effects. A Kemo VBF 35 system was used as a power supply, amplifier and anti-aliasing filter with a low-pass frequency fixed at 500 Hz for the measurements on the track and 250 Hz in the free field. The signals were recorded with an analog 14-channel TEAC tape recorder. The A/D conversion was performed using a 16 bit Daqbook 216 data acquisition system at a sampling rate of 1000 Hz.

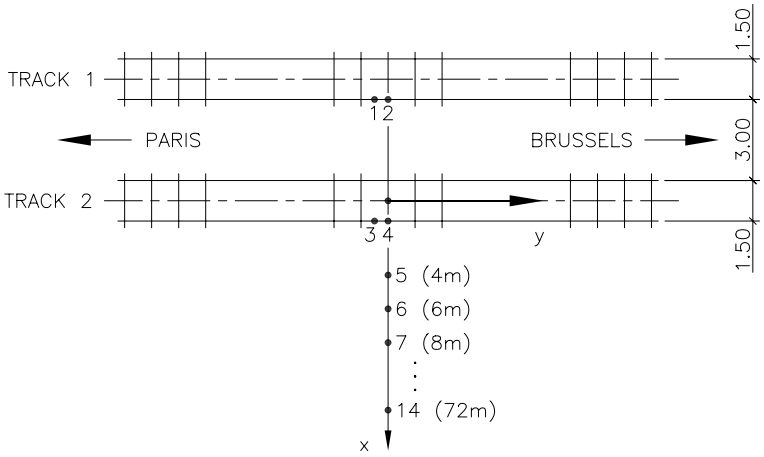

Figure 2: Location of the measurement points.

3 EXPERIMENTAL RESPONSE

9 train passages at speeds varying between 223 km/h and 314 km/h have been recorded. As an example, the track and free field response will be discussed in detail for the passage of the Thalys HST on track 2 with a speed $v = 314\,\text{km/h}$. Results for other train speeds are summarized afterwards, so that conclusions can be drawn regarding the influence of the train speed on the peak particle velocity (PPV).

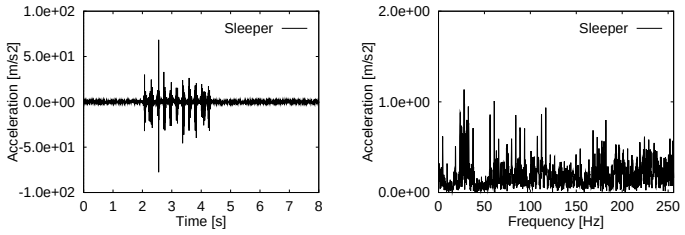

a. $a_z(Sleeper, t)$. *b.* $\hat{a}_z(Sleeper, \omega)$.

Figure 3: Measured time history (left) and frequency content (right) of the vertical acceleration of the sleeper during the passage of the Thalys HST on track 2 with a speed $v = 314\,\text{km/h}$.

3.1 *Track response*

Figure 3 shows the time history and frequency content of the vertical acceleration of the sleeper during the passage of the Thalys HST with a speed $v = 314\,\text{km/h}$. The time history clearly allows to identify the passage of all individual axles. The acceleration has a quasi-discrete spectrum (figure 3b) with peaks at the fundamental bogie passage frequency $f_b = v/L_b = 4.66\,\text{Hz}$ and its higher order harmonics, modulated at the axle passage frequency $f_a = v/L_a = 29.07\,\text{Hz}$.

3.2 *Free field response*

Figures 4 and 5 summarize the time history and frequency content of the free field vertical velocity at selected distances from the center of track 2, as obtained after integration of the measured accelerations.

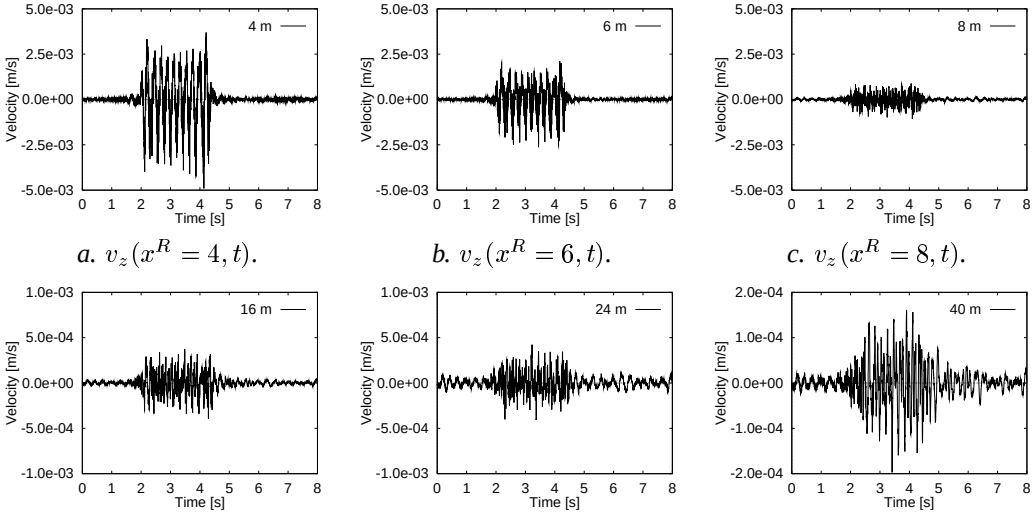

a. $v_z(x^R = 4, t)$. *b.* $v_z(x^R = 6, t)$. *c.* $v_z(x^R = 8, t)$.

d. $v_z(x^R = 16, t)$. *e.* $v_z(x^R = 24, t)$. *f.* $v_z(x^R = 40, t)$.

Figure 4: Measured time history of the vertical velocity in the free field for the passage of a Thalys HST on track 2 with $v = 314\,\text{km/h}$.

The time history of the vertical response $v_z(x^R = 6, t)$ at 6 m from the track (figure 4b), for example, still allows to detect the passage of the bogies, whereas the passage of the individual axles can no longer be distinguished. The PPV is about $2.5\,\text{mm/s}$. Due to the specific train composition, the observed velocity spectrum $\hat{v}_z(x^R = 6, \omega)$ (figure 5b) is quasi-discrete with a maximum at the fundamental bogie passage frequency $f_b = 4.66\,\text{Hz}$. The sleeper passage frequency $f_s = v/d = 145.37\,\text{Hz}$ is still noticeable in the spectrum.

The time history $v_z(x^R = 40, t)$ at 40 m from the track (figure 4f) has a PPV of about $0.2\,\text{mm/s}$.

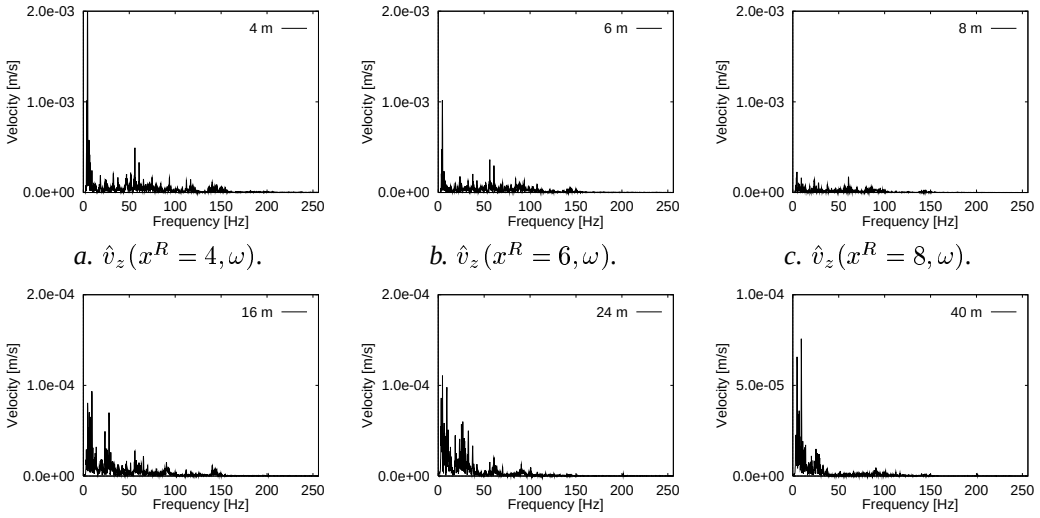

a. $\hat{v}_z(x^R = 4, \omega)$. *b.* $\hat{v}_z(x^R = 6, \omega)$. *c.* $\hat{v}_z(x^R = 8, \omega)$.

d. $\hat{v}_z(x^R = 16, \omega)$. *e.* $\hat{v}_z(x^R = 24, \omega)$. *f.* $\hat{v}_z(x^R = 40, \omega)$.

Figure 5: Measured frequency content of the vertical velocity in the free field for the passage of a Thalys HST on track 2 with $v = 314\,\text{km/h}$.

The velocity spectrum $\hat{v}_z(x^R = 40, \omega)$ (figure 5f) is dominated by the bogie passage frequency and its second harmonic. Higher frequencies are attenuated by radiation and material damping in the soil. The sleeper passage frequency, for example, can no longer be observed.

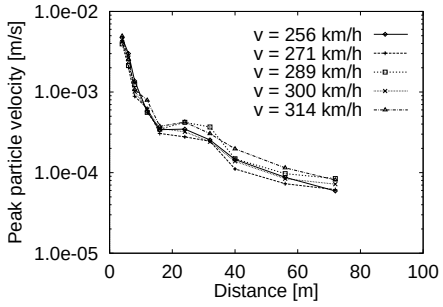

Figure 6: Measured PPV as a function of the distance to track 2 for Thalys HST passages on track 2 at different speed.

Figure 6 shows the PPV as a function of the receiver distance to track 2 for Thalys HST passages on track 2 at different speed. The decrease of PPV with distance due to radiation and material damping in the soil can clearly be observed. Figure 6 shows only a very moderate tendency of increasing vibration levels for increasing train speed.

4 KRYLOV'S ANALYTICAL PREDICTION MODEL

4.1 *Load distribution due to a train passage*

The track is modelled as a beam with bending stiffness EI and mass m per unit length on an elastic foundation with subgrade stiffness k_s. It is assumed that the track is directed along the y-direction, with the vertical z-axis pointing downwards, and the horizontal x-axis perpendicular to the (y, z)-plane (figure 7). The train has K axles; the load and the initial position of the k-th axle are denoted by T_k and y_k. A local coordinate $\xi = y - y_k - vt$ determines the position of a point y along the track with respect to the position $y_k + vt$ of the axle load. In this moving

frame of reference, the vertical deflection $w(\xi)$ of the track due to a single axle load T_k is equal to (Krylov 1998):

$$w(\xi) \quad = \quad \frac{T_k}{8EI\beta^3\delta} \exp\left(-\beta\delta \mid \xi \mid\right) \left(\cos\beta\eta\xi + \frac{\delta}{\eta} \sin\beta\eta \mid \xi \mid\right). \tag{1}$$

Herein, $\beta = (k_s/4EI)^{0.25}$, $\delta = [1 - (v/c_{min})^2]^{0.5}$ and $\eta = [1 + (v/c_{min})^2]^{0.5}$, with $c_{min} = (4k_sEI/m^2)^{0.25}$ the velocity of free track bending waves.

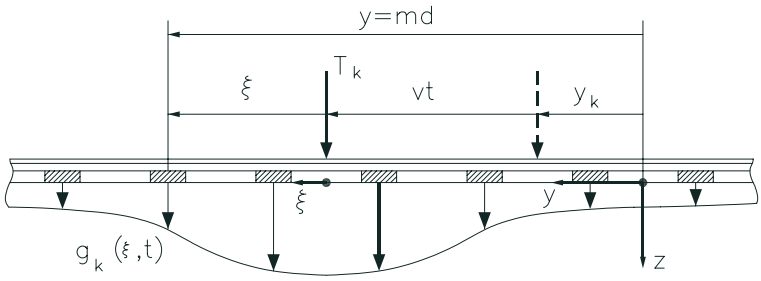

Figure 7: Vertical deflection curve of the track.

At time t, it is assumed that each sleeper m, located at $y = md$ (d is the sleeper distance) or $\xi = md - y_k - vt$, transfers a fraction of the axle load T_k proportional to its instantaneous deflection $w(\xi)$. The distribution of forces $g_k(\xi, t)$ can be written as the following summation:

$$g_k(\xi, t) \quad = \quad \frac{T_k}{N^{st}_{eff}} \frac{w(\xi)}{w^{st}_{max}} \sum_{m=-\infty}^{\infty} \delta(\xi + y_k + vt - md). \tag{2}$$

The Dirac function assures that, at time t when the axle load T_k is located at $y_k + vt$, the sleeper forces are transmitted at source locations $\xi = md - y_k - vt$ in the moving frame of reference. N^{st}_{eff} is the effective number of sleepers needed to support the axle load T_k, if all sleepers would take up a maximum load corresponding to the maximum quasi-static deflection $w^{st}_{max} = T_k/(8EI\beta^3\delta)$ of the track. N^{st}_{eff} is equal to $2y^{st}_0/\pi d$, with $y^{st}_0 = \pi/\beta$ the effective quasi-static track deflection distance. The Fourier transform of the distribution $g_k(\xi, t)$ is equal to:

$$\hat{g}_k(\xi, \omega) \quad = \quad \frac{1}{v} \frac{T_k}{N^{st}_{eff}} \frac{w(\xi)}{w^{st}_{max}} \left[\frac{2\pi v}{d} \sum_{m=-\infty}^{\infty} \delta(\omega - m\frac{2\pi v}{d})\right] \exp\left(i\omega\frac{\xi}{v}\right) \exp\left(i\omega\frac{y_k}{v}\right), \tag{3}$$

where the bracketed term is equal to the Fourier transform of a series of Dirac impulses, separated in time by d/v; it corresponds to a series of harmonics of the sleeper passage frequency v/d. The two last terms represent a phase shift.

The distribution of forces $D(\mathbf{x}, t)$ transmitted by all sleepers due to the passage of a train with K axles can now be written in the original coordinate system as:

$$D(\mathbf{x}, t) \quad = \quad \sum_{k=1}^{K} \int_{-\infty}^{\infty} \delta(x)\delta(y - \xi - y_k - vt)\delta(z) g_k(\xi, t)\, d\xi. \tag{4}$$

Introduction of expression (2) for $g_k(\xi, t)$ results in:

$$D(\mathbf{x}, t) \quad = \quad \sum_{k=1}^{K} \sum_{m=-\infty}^{\infty} \delta(x)\delta(y - md)\delta(z) \frac{T_k}{N^{st}_{eff}} \frac{w(md - y_k - vt)}{w^{st}_{max}}. \tag{5}$$

This expression is equivalent to the one proposed by Krylov. We prefer expression (4) to (5), however, as it can be used immediately in the Betti-Rayleigh reciprocity theorem applied to moving sources, as will be demonstrated in the following subsection. The Fourier transform of the distribution $D(\mathbf{x},t)$ is equal to:

$$\hat{D}(\mathbf{x},\omega) \quad = \quad \hat{F}(\omega)\hat{C}(\omega)\sum_{m=-\infty}^{\infty}\delta(x)\delta(y-md)\delta(z)\exp\left(-i\omega\frac{md}{v}\right). \tag{6}$$

The function $\hat{F}(\omega)$ represents the Fourier transform of the force transmitted by a single sleeper due to the passage of single unit axle load and follows immediately from the representation $\tilde{w}(k_\xi)$ of the deflection curve in the wavenumber domain with $k_\xi = \omega/v$:

$$\hat{F}(\omega) \quad = \quad \frac{1}{vN_{eff}^{st}}\frac{\tilde{w}(\omega/v)}{w_{max}^{st}} = \frac{1}{N_{eff}^{st}}\frac{1}{\beta v}\left[\frac{\delta+\eta+\frac{\omega}{v\beta}}{\delta^2+(\eta+\frac{\omega}{v\beta})^2}+\frac{\delta+\eta-\frac{\omega}{v\beta}}{\delta^2+(\eta-\frac{\omega}{v\beta})^2}\right]. \tag{7}$$

$\hat{F}(\omega)$ depends on the characteristics of the track, the subgrade stiffness k_s and the speed v of the train. The force transmitted by a sleeper is proportional to the sleeper distance d. The quasistatic value $\hat{F}(\omega=0)$ is independent on β or k_s, while it decreases for increasing v. The frequency content of $\hat{F}(\omega)$ increases for increasing k_s or β and increasing v. When v is much lower than c_{min}, the beam inertial forces can be neglected and δ and η tend to 1, resulting in the original expression of Krylov & Ferguson (1995) for low train speeds. The function $\hat{C}(\omega)$ represents the composition of the train in the frequency domain:

$$\hat{C}(\omega) \quad = \quad \sum_{k=1}^{K} T_k \exp\left(i\omega\frac{y_k}{v}\right). \tag{8}$$

4.2 *The free field response*

As the problem geometry is invariant with respect to y, the dynamic Betti-Rayleigh reciprocal theorem applied to moving loads can be used to write an efficient alternative for Krylov's original formulation (Lombaert & Degrande 2000). The free field vertical displacements are calculated as a convolution integral of $D(\mathbf{x},t)$ and the Green's function $u_{zz}^G(\mathbf{x},\mathbf{x}^R,t)$ of a layered halfspace, representing the vertical displacement component at a receiver $\mathbf{x}^R$ when a vertical force is applied at $\mathbf{x}$ (Degrande et al. 1998, Degrande 1999), resulting in:

$$u_z(\mathbf{x}^R,t) \quad = \quad \int_{-\infty}^{t}\int_{-\infty}^{+\infty}\sum_{k=1}^{K} u_{zz}^G(\mathbf{x}'^S,\mathbf{x}'^R,y^R-\xi-y_k-v\tau,t-\tau)g_k(\xi,\tau)\,d\xi\,d\tau, \tag{9}$$

where $\mathbf{x}'^S = \left\{x^S, z^S\right\}$ and $\mathbf{x}'^R = \left\{x^R, z^R\right\}$. As the source line is located at $x^S = 0$ and $z^S = 0$, the vector $\mathbf{x}'^S$ will be omitted in the following. The representation of the vertical displacements in the frequency-wavenumber domain is:

$$\tilde{u}_z(\mathbf{x}'^R,k_y,\omega) \quad = \quad \tilde{u}_{zz}^G(\mathbf{x}'^R,k_y,\omega)\int_{-\infty}^{+\infty}\sum_{k=1}^{K}\hat{g}_k(\xi,\omega-k_yv)\exp\left[ik_y(\xi+y_k)\right]d\xi. \tag{10}$$

Note that a frequency shift k_yv is applied to the argument of the force distribution $\hat{g}_k(\omega-k_yv)$, where ω is the frequency at the receiver, while $\omega-k_yv$ corresponds to the frequency emitted at the source. The latter will be denoted as $\tilde{\omega}$ in the following. The vertical soil displacements in the frequency domain are found as the inverse Fourier transform of equation (10):

$$\hat{u}_z(\mathbf{x}^R,\omega) \tag{11}$$

$$= \quad \frac{1}{2\pi v}\int_{-\infty}^{+\infty}\tilde{u}_{zz}^G(\mathbf{x}'^R,\frac{\omega-\tilde{\omega}}{v},\omega)\int_{-\infty}^{+\infty}\sum_{k=1}^{K}\hat{g}_k(\xi,\tilde{\omega})\exp\left[-i\frac{\omega-\tilde{\omega}}{v}(y^R-\xi-y_k)\right]d\xi\,d\tilde{\omega},$$

where a change of variables according to $k_y = (\omega - \tilde{\omega})/v$ has moved the frequency shift from the axle load to the transfer function. Accounting for the discrete spectrum (3) of the load distribution $\hat{g}_k(\xi, \tilde{\omega})$, this equation becomes:

$$\hat{u}_z(\mathbf{x}^R, \omega) = \left[\frac{1}{vN_{eff}^{st}} \frac{1}{w_{max}^{st}} \int_{-\infty}^{+\infty} w(\xi) \exp\left(i\xi \frac{\omega}{v}\right) d\xi\right] \left[\sum_{k=1}^{K} T_k \exp\left(i\omega \frac{y_k}{v}\right)\right]$$

$$\left[\frac{1}{d} \sum_{m=-\infty}^{+\infty} \tilde{u}_{zz}^G(\mathbf{x}'^R, \frac{\omega - m\frac{2\pi v}{d}}{v}, \omega) \exp\left[-i(\frac{\omega - m\frac{2\pi v}{d}}{v}) y^R\right]\right]. \quad (12)$$

This equation is equivalent to the final equation as derived by Krylov. The first two bracketed terms correspond to the functions $\hat{F}(\omega)$ and $\hat{C}(\omega)$ defined in equations (7) and (8), respectively. The third term is denoted as $\hat{u}_{\delta z}(\mathbf{x}^R, \omega)$ and is the desired alternative for Krylov's formulation: the original summation on the sleepers is replaced by a summation on integer multiples of the sleeper passage frequency v/d. The term $m = 0$ corresponds to a quasi-static contribution, while $|m| = +1$ corresponds to the sleeper passage frequency. Depending on the sleeper passage frequency, the speed of the train, the dynamic soil characteristics and the considered frequency range, the summation can be limited to a small number of harmonics, resulting in a considerable computational benefit.

The vertical soil displacements $u_z(\mathbf{x}^R, t)$ in the time domain are finally obtained by evaluating the inverse Fourier transform with a FFT algorithm.

5 ANALYTICAL PREDICTIONS

5.1 *Track response*

Calculations are made for a track with a bending stiffness $EI = 12.76 \times 10^6\,\text{Nm}^2$ (both rails) and a mass per unit length $m = 620.0\,\text{kg/m}$ (both rails and the sleepers). During the homologation tests, access to the track was limited to the time needed for the installation of the accelerometers on the rails and the sleepers. No forced vibration test on the track could be performed to measure the frequency dependent dynamic impedance of the track. Due to the lack of experimental data, subsequent calculations are made for a track with a constant subgrade stiffness $k_s = 250\,\text{MPa}$.

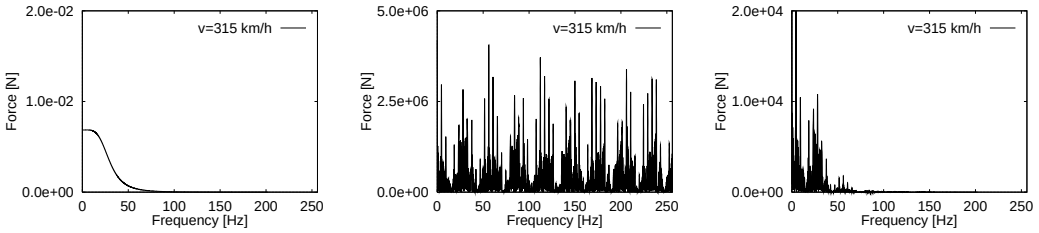

a. Modulus of $\hat{F}(\omega)$. *b. Modulus of $\hat{C}(\omega)$.* *c. Modulus of $\hat{F}(\omega)\hat{C}(\omega)$.*

Figure 8: Modulus of the functions (a) $\hat{F}(\omega)$, (b) $\hat{C}(\omega)$ and (c) $\hat{F}(\omega)\hat{C}(\omega)$ during the passage of a Thalys HST at a speed $v = 315\,\text{km/h}$.

Figures 8a and 8b show the moduli of $\hat{F}(\omega)$ and $\hat{C}(\omega)$ for a Thalys HST moving at a speed $v = 315\,\text{km/h}$. The quasi-static value $\hat{C}(\omega = 0)$ is equal to the sum of all axle loads. As the locomotives and the side carriages of the Thalys HST have a different axle composition than the 6 central carriages, the spectrum is quasi-discrete with peaks at the fundamental bogie passage frequency $f_b = 4.66\,\text{Hz}$ and its higher order harmonics, modulated at the axle passage frequency

$f_a = 29.07\,\text{Hz}$ (figure 8b). Note that the measured vertical acceleration of a sleeper has a similar quasi-discrete spectrum (figure 3d). The spectrum in figure 8c is obtained as the product of $\hat{F}(\omega)$ and $\hat{C}(\omega)$ and represents the frequency content of the force transmitted by a single sleeper during the passage of a Thalys HST. The decay of the function $\hat{F}(\omega)$ with frequency governs the frequency content of the transmitted load.

5.2 *Free field response*

The vertical displacement $\hat{u}_z(\mathbf{x}^R, \omega)$ at a receiver is obtained by evaluation of equation (12). The first two terms in this equation have been illustrated already in figure 8. The Green's functions of the layered halfspace are calculated with a direct stiffness formulation for wave propagation in multilayered poroelastic media (Degrande et al. 1998). Figure 9a shows a contour plot of the Green's function $\tilde{u}^G_{zz}(\mathbf{x}'^R, \overline{k}_y, \omega)$ for $x^R = 16\,\text{m}$ and $z^R = 0$ as a function of the dimensionless wavenumber $\overline{k}_y = k_y C_s/\omega$ and the frequency ω. Superimposed on the same plot are the branches of the absolute value of the dimensionless wavenumber $\overline{k}_y = [(\omega - \tilde{\omega})/v]C_s/\omega$ for $\tilde{\omega} = m2\pi v/d$. The quasi-static contribution ($m = 0$) corresponds to $\overline{k}_y = C_s/v$. The third term $\hat{u}_{\delta z}(\mathbf{x}^R, \omega)$ in equation (12) is presented in figure 9b and is obtained as the intersection of the previous branches with the Green's function. These figures illustrate that the required number of harmonics depends on the speed of the train, the soil velocities and the sleeper passage frequency.

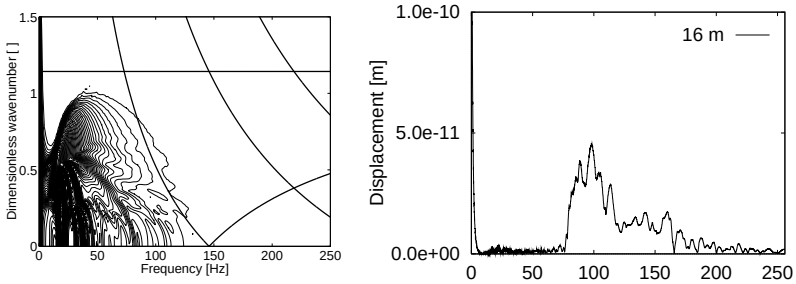

a. $\tilde{u}^G_{zz}(\mathbf{x}'^R, \overline{k}_y, \omega)$. *b.* $\hat{u}_{\delta z}(\mathbf{x}^R, \omega)$.

Figure 9: (a) Modulus of the Green's function $\tilde{u}^G_{zz}(\mathbf{x}'^R, \overline{k}_y, \omega)$ as a function of $\overline{k}_y$ and ω and (b) of the function $\hat{u}_{\delta z}(\mathbf{x}^R, \omega)$ for $x^R = 16\,\text{m}$ and $z^R = 0$.

Figures 10 and 11 show the computed time history and the frequency content of the vertical velocity at selected receivers during the passage of a Thalys HST at 314 km/h. These results should be compared with the experimental data, presented in figures (4) and (5), respectively.

At 4 m from the track, the passage of the bogies can be observed, while the passage of the individual axles is no longer observable; this is true for the observed (figure 4a) and predicted (figure 10a) velocity time history. While the predicted PPV has the same order of magnitude as the measured one, the time history clearly shows that the frequency content of the predicted response differs from the measured spectrum. The observed velocity spectrum (figure 5a) is quasi-discrete, with a maximum at the fundamental bogie passage frequency $f_b = 4.66\,\text{Hz}$. A similar behaviour can be observed at low frequencies in the predicted spectrum (figure 11a), although the contribution at the fundamental bogie passage frequency is underestimated. This is due to high-pass frequency filtering introduced by the assumed soil stratification. The predicted spectrum has low amplitudes between 30 and 75 Hz, while the frequency components around the sleeper passage frequency $f_d = 145.37\,\text{Hz}$ are more pronounced. This is caused by the fact that Krylov's prediction model only includes the effect of quasistatic loading and sleeper passage, while other excitation mechanisms are not accounted for. The model also overestimates the sleeper passage effect at high frequencies, as the sleeper forces are transmitted as point forces, an assumption that

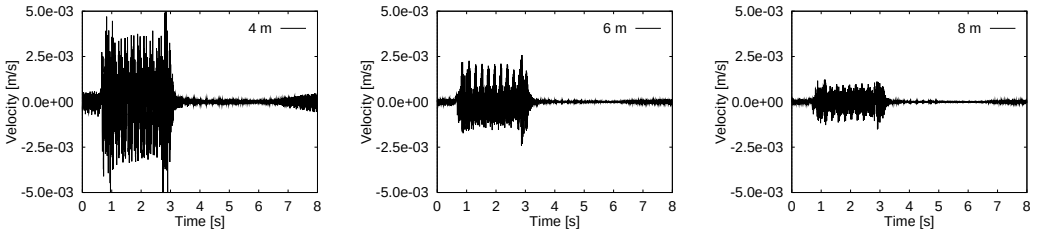

a. $v_z(x^R = 4, t)$. *b.* $v_z(x^R = 6, t)$. *c.* $v_z(x^R = 8, t)$.

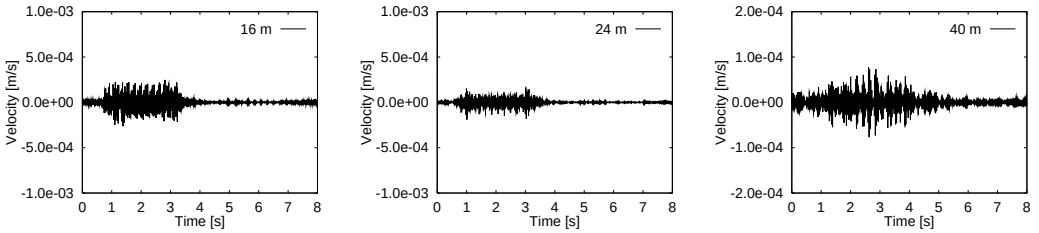

d. $v_z(x^R = 16, t)$. *e.* $v_z(x^R = 24, t)$. *f.* $v_z(x^R = 40, t)$.

Figure 10: Computed time history of the vertical velocity at varying distances from the track during the passage of a Thalys HST at $v = 314\,\text{km/h}$.

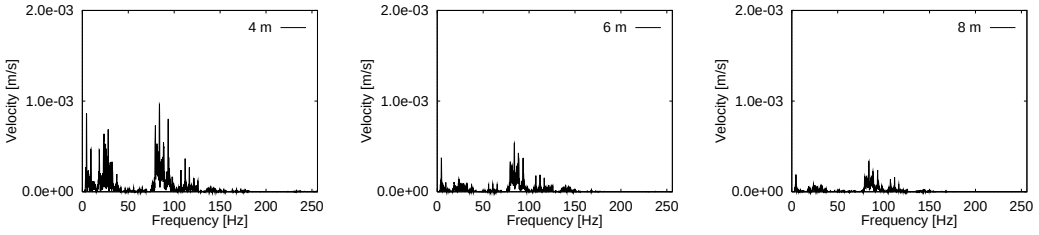

a. $\hat{v}_z(x^R = 4, \omega)$. *b.* $\hat{v}_z(x^R = 6, \omega)$. *c.* $\hat{v}_z(x^R = 8, \omega)$.

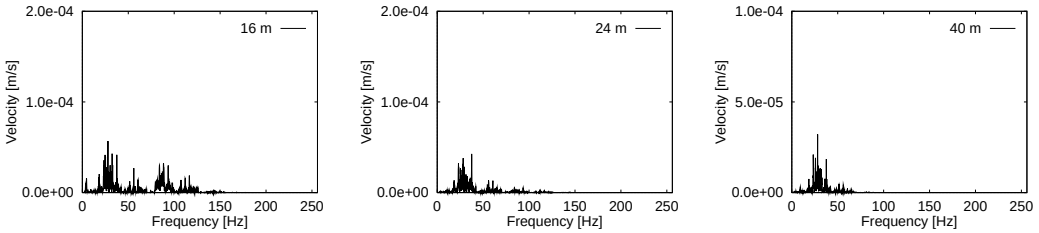

d. $\hat{v}_z(x^R = 16, \omega)$. *e.* $\hat{v}_z(x^R = 24, \omega)$. *f.* $\hat{v}_z(x^R = 40, \omega)$.

Figure 11: Computed frequency content of the vertical velocity at varying distances from the track during the passage of a Thalys HST at $v = 314\,\text{km/h}$.

is challenged when the frequency increases and the wavelenghts in the soil have the same order of magnitude as the sleeper dimensions.

The PPV at 16 m from the track is about 0.25 mm/s (figure 10d) and corresponds well with the measured PPV (figure 4d). The predicted time history reveals, however, that its frequency content is too high. The measured velocity spectrum (figure 5d) is dominated by the bogie passage frequency and its second harmonic. Higher frequencies are attenuated by radiation and material damping in the soil. The predicted velocity spectrum (figure 11d) is more pronounced around 25 Hz, while low frequency components are much lower. This is due to the assumed stratification of the soil, which introduces filtering of frequencies below 15 Hz. The predicted frequency content is much higher than the observed. Apart from the overestimation of the response at frequencies related to sleeper passage, this also indicates that a material damping ratio $\beta = 0.03$ underesti-

mates the damping in the top layers. Comparing the measured and predicted response at larger distances reveals that the reverse is true for the deeper layers.

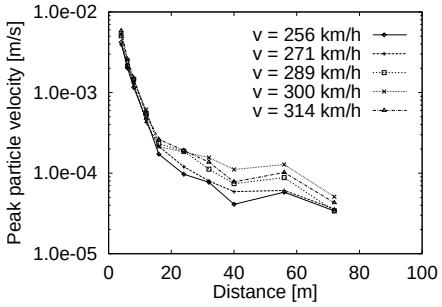

Figure 12: Computed PPV as a function of distance and train speed.

Figure 12 finally summarizes the PPV at all points in the free field for the 5 train passages on track 2. The decrease of PPV with distance due to radiation and material damping in the soil is apparent. The experimental results of figure 6 demonstrate a rather weak dependence of PPV on train speed, whereas this dependence is more pronounced in the numerical results (figure 12); although PPV are predicted with rather good accuracy, it has been demonstrated before that the same is not true regarding the frequency content of the response.

6 CONCLUSION

The results of free field vibration measurements during the passage of a Thalys HST at varying speed have been compared with numerical results obtained with an efficient alternative formulation of Krylov's prediction model. The experimental data presented in this paper are complementary to other data sets published in literature. Especially the fact that measurements have been made at 9 different train speeds between 223 km/h and 314 km/h, makes this data set unique.

A major shortcoming of the present data set is that, due to time and budget limitations, no in situ experiments have been made to determine the subgrade stiffness of the track. Only limited data are also available on the stratification of the soil and the variation of dynamic soil characteristics with depth, especially material damping. This compromises the quantitative validation of numerical prediction models.

Instead of trying to match the experimental results by modifying the input parameters in a 'trial and error' procedure, a qualitative assessment of the predictions has been made. The model has proven good predictive capabilities at low (quasistatic) and high frequencies (sleeper passage frequency and its higher harmonics), but seems to underestimate the response in the mid-frequency band. Apart from incomplete input data, this is due to the fact that the model only incorporates quasi-static loading, while dynamic loading due to rail and wheel irregularities, for example, are disregarded. Our present research concentrates on the development of a prediction model that accounts for different excitation mechanisms and through-soil coupling of the sleepers.

ACKNOWLEDGEMENTS

The in situ experiments have been performed in cooperation with L. Schillemans of Technum and with the assistance of K. Peeraer. The collaboration of P. Godart and W. Bontinck of the NMBS is kindly acknowledged. W. Dewulf inverted the SASW data. Prof. Krylov of Nottingham Trent University is gratefully acknowledged for the interesting discussions on the theory and the numerical results.

REFERENCES

Adolfsson, K., Andréasson, B., Bengtson, P.-E., Bodare, A., Madshus, C., Massarch, R., Wallmark, G. & Zackrisson, P. (1999), High speed lines on soft ground. Evaluation and analyses of measurements from the West Coast Line, Technical report, Banverket, Sweden.

Auersch, L. (1989), Zur Entstehung und Ausbreitung von Schienenverkehrserschutterungen - theoretische Untersuchungen und Messungen an Hochgeschwindigkeitszug Intercity Experimental, Forschungsbericht 155, Bundesanstalt für Materialforschung und -prüfung, Berlin.

Branderhorst, J. (1997), Modellen voor het boeggolfprobleem bij hogesnelheidstreinen. Ontwerp en validatie met behulp van de resultaten van de proef Amsterdam-Utrecht, Master's thesis, Universiteit Twente, Holland Railconsult.

Degrande, G. (1999), Free field vibrations during the passage of a high speed train: validation of a numerical model by means of experimental results, *in* P. Jones & R. Ghanem, eds, '13th ASCE Engineering Mechanics Division Specialty Conference', Baltimore, MD, USA. CD-ROM.

Degrande, G. (2000), Free field vibrations during the passage of a high speed train: experimental results and numerical predictions, *in* V. Krylov, ed., 'Noise and vibration from high-speed trains', Thomas Telford Publishing, London, pp. 1–28. Accepted for publication.

Degrande, G., De Roeck, G., Van den Broeck, P. & Smeulders, D. (1998), 'Wave propagation in layered dry, saturated and unsaturated poroelastic media', *International Journal of Solids and Structures* **35**(34-35), 4753–4778. Poroelasticity Maurice A. Biot memorial issue.

Degrande, G. & Schillemans, L. (1998), Free field vibrations during the passage of a HST, *in* P. Sas, ed., 'Proceedings ISMA 23, Noise and Vibration Engineering', Vol. III, Leuven, Belgium, pp. 1563–1570.

Dewulf, W., Degrande, G. & De Roeck, G. (1996), Spectral analysis of surface waves: an automated inversion technique based on a Gauss-Newton inversion algorithm. Conference on Inverse Problems of Wave Propagation and Diffraction, Aix-les-Bains, France.

Knothe, K. & Wu, Y. (1998), 'Receptance behaviour of railway track and subgrade', *Archive of Applied Mechanics* **68**, 457–470.

Krylov, V. (1994), 'On the theory of railway-induced ground vibrations', *Journal de Physique IV* **4**(C5), 769–772.

Krylov, V. (1995), 'Generation of ground vibrations by superfast trains', *Applied Acoustics* **44**, 149–164.

Krylov, V. (1998), 'Effects of track properties on ground vibrations generated by high-speed trains', *Acustica-Acta Acustica* **84**(1), 78–90.

Krylov, V. & Ferguson, C. (1995), 'Recent progress in the theory of railway-generated ground vibrations', *Proceedings of the Institute of Acoustics* **17**(4), 55–68.

Lombaert, G. & Degrande, G. (2000), An efficient formulation of Krylov's prediction model for train induced vibrations based on the dynamic reciprocity theorem, *in* '7th International Congress on Sound and Vibration', Garmisch-Partenkirchen, Germany. Submitted for publication.

Van den Broeck, P. & De Roeck, G. (1996), Dynamic behaviour of railway track on layered media, *in* G. Augusti, C. Borri & P. Spinelli, eds, 'Proceedings of the 3rd European Conference on Structural Dynamics: Eurodyn '96', A.A. Balkema, Rotterdam, Florence, Italy, pp. 1083–1089.